ELSEVIER

International Journal of Mass Spectrometry 219 (2002) 381–389

International Journal of Mass Spectrometry

www.elsevier.com/locate/ijms

Threshold photoelectron spectroscopy with velocity focusing: an ideal match for coincidence studies

Tomas Baer*, Yue Li

Department of Chemistry, University of North Carolina, Chapel Hill, NC 27599-3290, USA

Received 18 December 2001; accepted 8 February 2002

Abstract

Velocity focusing of low energy electrons has been used to collect threshold photoelectron spectra with a continuous tunable vacuum UV light source. Velocity focusing permits focusing the photoionization image from 5 mm × 8 mm to 1 mm × 1 mm, and thus to collect threshold electrons (less than 10 meV) with a collection efficiency close to 50%. The overall resolution for Xe^+ of 13 meV is limited primarily by the 12 meV band pass of the photon monochromator. The collection efficiency for energetic electrons of 1 eV is reduced 0.07%. This method of detecting threshold electrons has improved the resolution by a factor of 4 and increased the signal by a factor of 10. It is an ideal approach for photoelectron photoion coincidence (PEPICO) studies because it permits the collection of electrons and ions with relatively high electric fields of 20 V/cm, which are necessary to have narrow time of flight peaks for the coincident ion signals. (Int J Mass Spectrom 219 (2002) 381–389)

Keywords: Velocity focusing; Photoelectron photoion coincidence; Photoelectron spectroscopy; Photoionization

1. Introduction

Photoelectron photoion coincidence (PEPICO) spectroscopy has long been a major method for determining the dissociation dynamics of energy-selected ions and the determination of accurate ion thermochemistry [1–9]. Because high collection efficiencies for both ions and the energy-selected electrons is essential in coincidence studies, the detection of threshold electrons with their accompanying high collection efficiency has been an attractive approach for PEPICO studies. PEPICO studies can only be carried out with continuous light sources so that single ionization events can be correlated. Threshold electrons can be energy analyzed by passing the electrons through small apertures so that electrons with off-axis velocity components are stopped by the apertures [10–12]. Thus, the resolution is based solely on the angular discrimination against energetic electrons. A resolution of 20 meV is routinely achieved by this approach. However, these energy analyzers have always suffered from the fact that energetic (or hot) electrons, whose initial velocity is in the direction of the electron detector, pass through the small apertures and are collected along with the true threshold electrons. Thus, the analyzer function for threshold electrons is asymmetric and contains a long tail that never goes to zero. The use of pulsed synchrotron light has permitted the elimination of this hot electron tail by electron TOF discrimination against the energetic electrons

* Corresponding author. E-mail: baer@unc.edu

1387-3806/02/$ – see front matter
PII S1387-3806(02)00694-2

[13,14]. The resolution improved to 5 meV. However, single bunch operation of modern synchrotrons is not a practical use of the beam current and thus tends to be discouraged. Thus, improved methods for using continuous light sources with threshold electron detection continue to be important.

A major advance in the high-resolution detection with quasi-continuous light was the development of pulsed field ionization (PFI) in which high-*n* Rydberg states are prepared by the VUV light and then ionized by the application of a small (0.5 V/cm) pulse [15]. Not only does this provide a means for high-resolution ion spectroscopy, but the hot electron tail is completely eliminated. In addition, it also allows for PEPICO studies with high resolution, an experiment not possible with pulsed lasers [16,17]. The major disadvantages of PFI detection and PFI–PEPICO studies is low signal levels and the fact that they cannot be increased by degrading the resolution. Thus, any method that can increase the signal level and provide suppression of hot electrons is welcome.

The traditional approach to threshold electron detection is posited on the extraction of zero energy electrons in parallel trajectories toward the aperture in front of the electron collector. To ensure parallel trajectories, the electrostatic extraction fields must be very uniform in order to avoid lensing. In such an analyzer, the electron resolution is inversely related to the applied extraction field. Unfortunately, low electric fields make it difficult to extract the ions with good efficiency and narrow time of flight widths. An alternative approach to threshold electron detection is the penetrating field method [18,19] in which a very small electric field ($\ll$1 V/cm) is applied to the photoionization region to gently extract the low energy electrons and focus them through a small hole. However, this method suffers from the same problem with respect to efficient ion extraction. The discovery of velocity map imaging by Chandler and Parker [20,21] has turned all this up side down because the requirements for high electron resolution and efficient ion extraction are no longer contradictory. Rather than installing grids, the electrons and ions are extracted through large apertures with no grids so that they are focused in such a manner that the zero energy electrons (or ions) are focused to a spot on the detector, while electrons with velocities perpendicular to the extraction axis are focused into concentric rings around the central spot. This velocity map imaging has greatly improved the resolution provided by imaging detectors. Because the resolution is highest for the low energy electrons, it is apparent that such an approach is also ideal for the detection of threshold electrons. Of major interest is the fact that an extended photoionization image can be focused down to a very small spot. In addition, the electric field that extracts the electrons and ions can be very large. We have thus adapted our threshold PEPICO experiment by installing such a velocity focusing electron extraction lens, and present here the first results.

2. Experimental approach

The experimental set-up is shown in Fig. 1. Electrons are extracted in a field of 20 V/cm and further accelerated by a second plate to 60 V in the drift tube. This voltage was obtained by optimizing the signal level and resolution, using the voltages suggested by SIMION [22] modeling of the electron trajectories as the starting point. The SIMION calculations suggested a voltage of 56 V for the drift tube. Because the electrons are focused to a very small hole with a diameter of 1.4 mm, four deflection plates were installed in the drift tube so that the threshold electrons could be optimally focused onto the exit aperture. When the steering plates were set about 2 V above or below the drift tube voltage, the signal improved by about a factor of two. The skimmer placed near the end of the drift tube was installed to minimize the number of scattered high-energy electrons that might reach the electron detector. It is not certain, how important this skimmer is in suppressing the scattered electrons.

The photoionization image in our experiment is estimated to be about 5 mm high, while the 2 mm thickness of the region is determined by the *f* value of the photon monochromator and the 2 cm distance

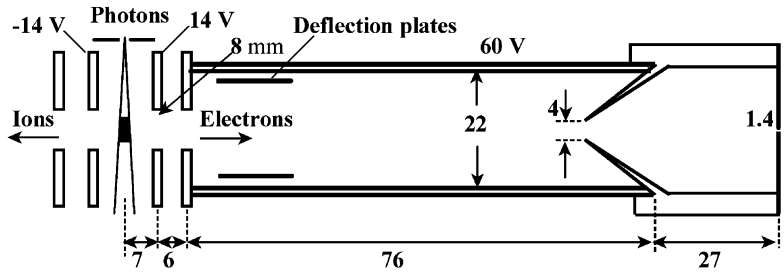

Fig. 1. The electron velocity focusing optics used to collect the threshold photoelectron spectrum. The drawing is approximately to scale with dimensions in milimeter.

of the ionization region from the optical slit of the photon monochromator. Because the photon beam traverses the whole ionization region, the effective width of the photoionization region is determined by the 8 mm apertures in the electron and ion extraction plates. Thus, the 2 mm × 5 mm × 8 mm volume of the photoionization region must be focused down to the 1.4 mm final aperture.

Fig. 2 shows the results of SIMION simulations for several electron energies and different starting positions (perpendicular to the extraction field) in the ionization region. It is evident that initially zero energy electrons can be focused to a spot on the detector that is independent of the starting position up to about 1.5 mm from the axis. Even when the electron starts 3 mm from the axis, it will hit the detector in a radius of less than 0.5 mm. On the other hand, 5 meV electrons hit the detector about 1.5 mm from the center. The effectiveness of focusing energetic electrons over an extended source region is clearly less than it is for initially zero energy electrons. This fact, combined with the closer spacing of the energetic electrons at

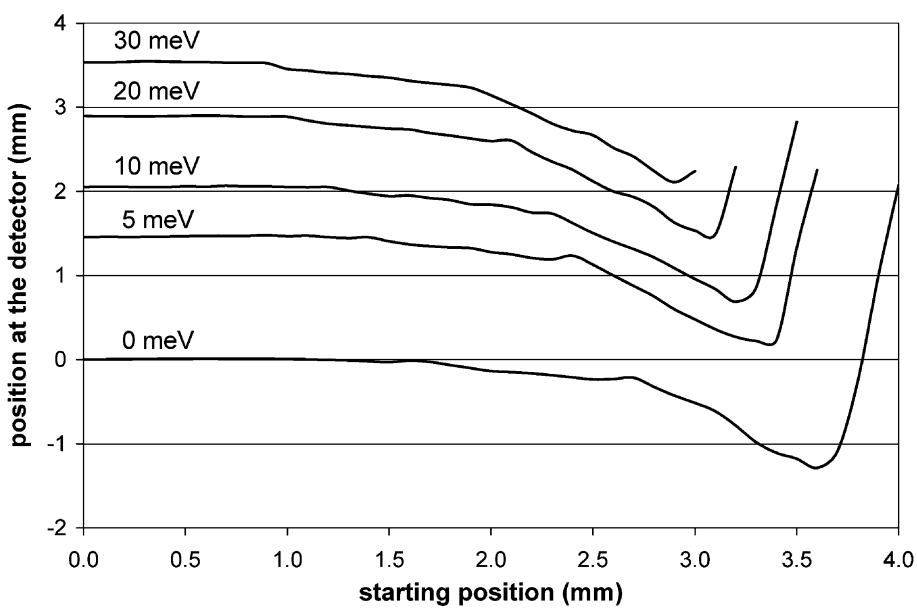

Fig. 2. SIMION electron trajectory calculations, showing the focusing of 0, 5, 10, 20, and 30 meV electrons as a function of their starting position (perpendicular to the extraction axis).

the detector means that the resolution drops rapidly with increasing electron energy.

Unfortunately, this imaging approach does not affect the trajectory of energetic electrons whose initial velocity is in the direction of the extraction field. Even electrons originating from the 5 mm ionization region with 1 eV of energy in the direction of the detector are focused into the center of the plate. This means that energetic electrons initially directed toward the detector are not stopped by this velocity focusing analyzer.

3. Threshold photoelectron spectra (TPES) and photoelectron photoion coincidence (PEPICO) spectra

Fig. 3 shows the photoelectron spectrum of Xe obtained with a photon monochromator resolution of 12 meV. The resulting total resolution of the first peak is 13 meV. If we deconvolute the photon resolution from this peak, we deduce that the actual electron energy resolution is on the order of about 5 meV. The overall resolution is clearly limited by the photon monochromator. Our set-up is not optimized for high resolution because the photon monochromator is only a 1-meter instrument with a practical limit of about 1 Å or 12 meV (at 1000 Å) resolution.

The shape of the photelectron peak is typical of threshold photoelectron peaks in that the peak rises with a resolution given by the photon monochromator, but falls with a slight tailing due to the discrimination against energetic electrons, which increases with increasing electron energy. At 0.08 eV, the collection efficiency drops to 2.8% of its value at zero energy, and by 0.4 and 1 eV this value drops to 0.6 and 0.17%, respectively. These efficiencies are determined by normalizing the electron signal by the total ion signal. Not taken into account is the angular distribution of the photoelectrons, which in fact varies enormously ($1 > \beta > -1$) over the energy range shown in Fig. 3

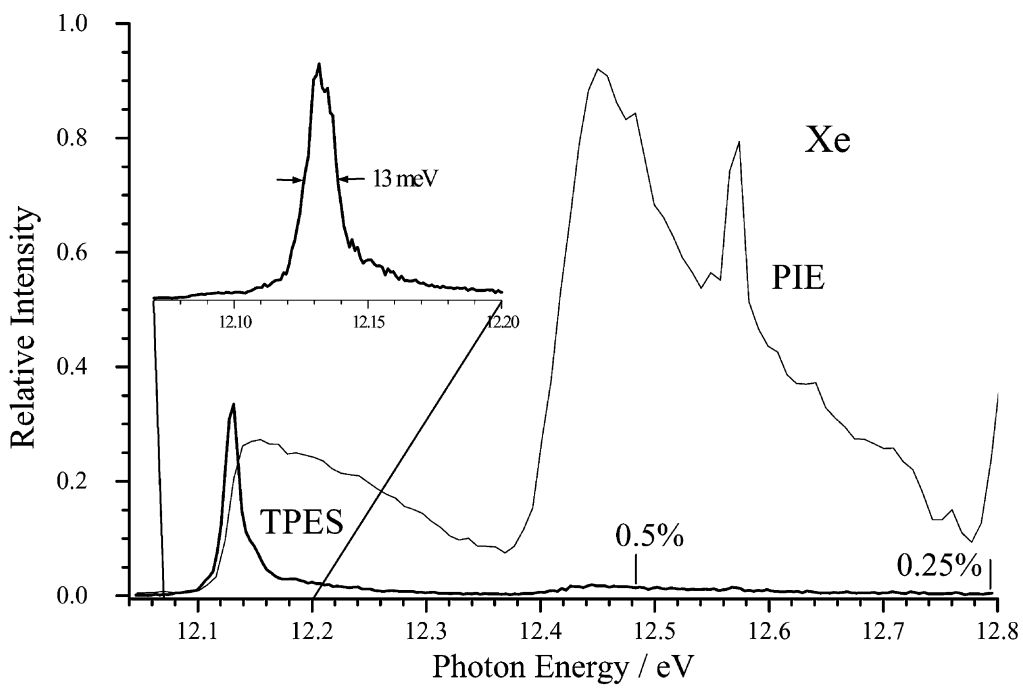

Fig. 3. The threshold photoelectron spectrum of Xe obtained with the velocity focusing optics and the total ion signal, the photoionization efficiency (PIE) spectrum. The inserted TPES near the ionization energy was obtained with increased step size of 1 meV per point with a collection time of 15 s per point.

[23]. We tried to choose energies at which the angular distribution is isotropic ($\beta = 0$) for the determination of this efficiency but because β changes vary rapidly with energy, this approach is only partially successful. We expect that these efficiencies are accurate within 50% of their value.

At very high electron energies ($E \gg 20$ eV), the only electrons that pass through the 1.4 mm exit hole are ones whose initial velocity vector is directed to that hole. Thus, the limiting value of the collection efficiency is given by the area of the exit hole divided by the area of the sphere with a radius of 116 mm, which is about 0.004% The radius of 116 mm is simply the distance from the ionization region to the electron exit hole. This simple calculation assumes that the electrons are ejected isotropically. Furthermore, it ignores the fact that electrons formed at positions significantly off the axis are not focused onto the hole, which means that energetic electrons formed at those positions will pass through the hole, thereby affecting the discrimination against hot electrons.

The spectrum in Fig. 3 shows that the resolution for threshold electrons with velocity focusing is quite respectable. However, the much bigger advantage of this approach is the increased signal level. The fact that the full image can be demagnified to a spot size of 1.4 mm means that such an analyzer is an ideal match for PEPICO experiments. One of the properties of the PEPICO experiment is the ability to determine absolute collection efficiencies for both electrons and ions [24,25]. If $E\ell$ = electron c/s, I = ion c/s, and C = coincidence c/s, then the collection efficiency for electrons and ions is given by:

$$\text{Electron Collection Efficiency} = \frac{C}{I} \quad (1)$$

$$\text{Ion Collection Efficiency} = \frac{C}{E\ell} \quad (2)$$

Count rates at the Xe $^2P_{3/2}$ peak at 12.130 eV were 113 electrons/s, 45 ions/s, and 22 coincidences/s. This yields electron and ion collection efficiencies of 49% and 20%, respectively. This represents more than a

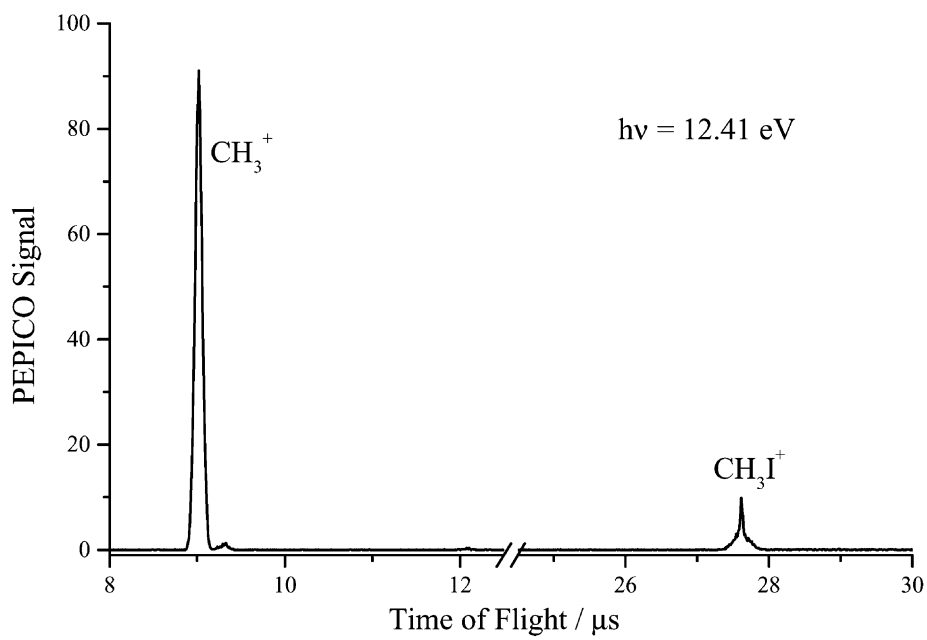

Fig. 4. The photoelectron photoion coincidence mass spectrum of CH_3I in the vicinity of the dissociative ionization onset. The small peak to the right of the CH_3^+ peak at 9 μs is due to the ^{13}C isotope. The two-component shape of the parent ion peak at 17.6 μs is a result of the effusive jet that gives rise to the sharp peak on top of the thermal background peak.

10-fold increase in electron signal from our previous electron extraction system.

The collection efficiency is important in coincidence experiments because of background noise due to false coincidences. Fig. 4 shows a coincidence time-of-flight (TOF) mass spectrum of methyl iodide obtained at a photon energy near this ion's dissociation limit to CH_3^++I. At this energy, the total ion and electron rates were 100 and 1.6 c/s, respectively, while the coincidence count rate was 0.47 c/s. (The low electron collection efficiency is a result of the low production rate of threshold electrons at this photon energy.) The false coincidence rate in a given time interval, ΔT, is given by:

$$\text{False coincidence rate} = E\ell \times I \times \Delta T \tag{3}$$

The signal to noise ratio is then given by:

$$\text{Signal to noise} = \frac{C}{(E\ell \times I \times \Delta T)} = \frac{\text{Ion Collection Efficiency}}{I \times \Delta T} = \frac{\text{Electron Collection Efficiency}}{E\ell \times \Delta T} \tag{4}$$

Thus, the higher the collection efficiencies for ions and electrons, the greater will be the signal to noise. In addition, the narrower the TOF peak (ΔT), the higher the signal to noise ratio. Narrow TOF peaks are associated with high electric draw-out fields. Thus, an advantage of the velocity focusing optics is that they work very well with relatively high draw-out fields. The false coincidence background in Fig. 4 is about 15 c/μs. This spectrum was collected overnight for total time of 53,000 s in order to collect a statistically significant number of false electrons. The CH_3^+TOF peak has a width at its base of about 0.27 μs. Thus, the false coincidence background under the methyl ion TOF peak is just 4 c/s, compared to the total counts of 22,000 counts, for a signal to noise of about 5500. We can calculate the theoretical false coincidence background by substituting into the above equation. This yields a false coincidence background in the 0.27 μs of 2.3 c/s, which is within a factor of two equal to the observed false background rate of 4 c/s.

4. Application to the dissociation of methyl iodide

Fig. 5 shows the breakdown diagram for methyl iodide obtained by plotting the relative abundance of the coincident CH_3^+ and CH_3I^+ ion signals. This molecule was chosen because it has little thermal energy at room temperature and it dissociates rapidly at its dissociation limit, thus avoiding the problems associated with a kinetic shift. The points were obtained from TOF mass spectra (as in Fig. 4). The solid lines are calculated by assuming that any ion with an energy above its dissociation limit will fragment, and convoluting this step function with the CH_3I thermal energy distribution. If the sample methyl iodide had no internal energy (i.e., $T = 0$ K), the breakdown diagram would take the form of step functions at the dissociation limit in which the parent ion drops from 1.0 to 0.0 and the daughter ions increases to 1.0. The slow rise on the low energy side is determined by the molecule's thermal energy distribution, in this case consisting almost entirely of rotational energy. It is evident that assumed temperature of 298 K underestimates the production of CH_3^+ products at low energies. A similar finding was noted in recent pulsed field ionization PEPICO experiments, in which this effect was attributed to the favored production of fragment ions because the dissociation event stabilizes the high-*n* Rydberg states that ultimately generate the threshold electrons [26,27]. That is, the photon absorption initially produces a superexcited Rydberg state, CH_3I^*, which can decay via several paths including dissociation to neutral fragments, ejection of an energetic electron to produce ground state ions, and by the production of a threshold electron. The latter path represents only a few percent of the total decay routes. Thus, if the dissociation of the ion core perturbs the Rydberg electron causing it to form a stable high-*n* state, the production of a threshold electron will be favored. Evidence for such an enhancement for the case of CH_3I was presented by Song et al. [28] We can account for this by multiplying the expected CH_3^+ signal by a variable factor (*f*) until the data are fitted. This best fit is obtained with a factor $f = 3$.

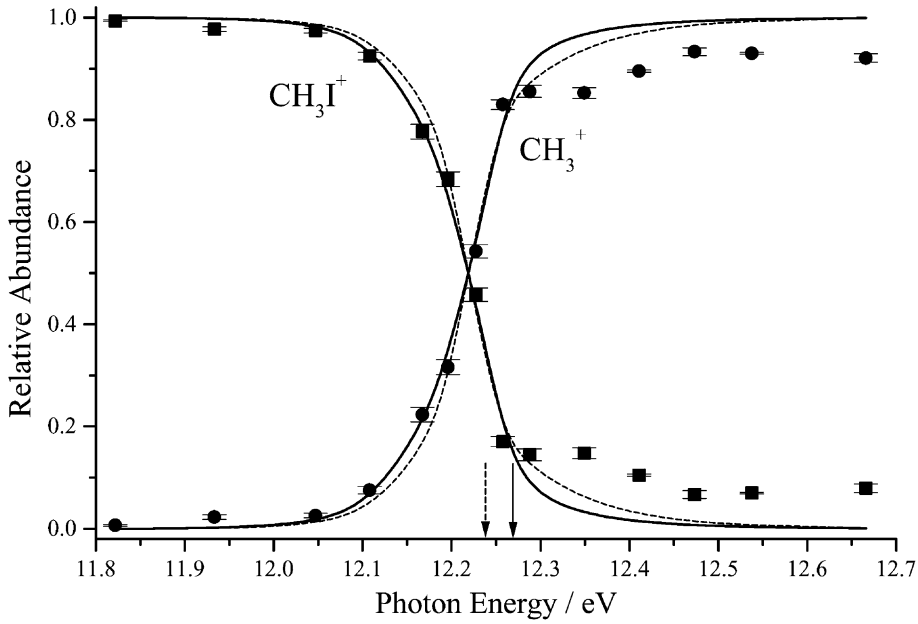

Fig. 5. The threshold photoelectron photoion coincidence breakdown diagram for CH_3I obtained with the velocity focusing optics. The dashed line is the calculated breakdown diagram in which the production of threshold electrons is independent of the ion core dissociation. The solid line assumes that the dissociative core favors the production of threshold electrons by a factor of three, thereby enhancing the fragment ion signal. The resulting 0 K dissociation limits are 12.238 and 12.268 eV, respectively.

The vertical arrows indicate the measured 0 K dissociation limits, which we find to be 12.230 eV when $f = 1$ and 12.268 when $f = 3$. This adjustment not only fits the low energy part of the breakdown diagram, but it also brings the derived dissociation limit to the thermochemically expected onset energy. The improved resolution of the velocity focusing optics is providing us for the first time the ability to detect this increased efficiency for threshold electron production accompanied by a dissociating ionic core (Table 1).

Table 1
0 K Appearance Energies of CH_3^+ from CH_3I

CH_3^+ AE (eV)	Method
12.256	Thermochemistry[a]
12.269	PFI-PEPICO[b]
12.266	Photodissociation[c]
12.238	This work with no correction
12.268	This work with correction[d]

[a] Based on $\Delta_f H_0^\circ(CH_3I) = 23.9$ kJ/mol, [29] $\Delta_f H_0^\circ(CH_3^+) = 1099.1$ kJ/mol, [26] and $\Delta_f H_0^\circ(I) = 107.2$ kJ/mol [30].
[b] Pulsed field ionization PEPICO study by Song et al. [28].
[c] Walter et al. [31].
[d] Analysis included increased threshold electron production associated with dissociating ionic core.

5. Toward the elimination of the "hot electron tail"

While the velocity focusing improves resolution and collection efficiency, it does not completely eliminate the hot electron contribution to the coincidence signal, which is caused by energetic electrons that have their initial velocity vector directed at the electron detector. In fact, this tail is evident in Fig. 5, where the parent ion signal does not drop to the baseline above the dissociation limit. Because of the very large number of CH_3I^+ ions formed (the ionization energy of 9.5 eV is nearly 3 eV below the dissociation limit), the fraction of threshold electrons is very small. Three approaches have been tried to reduce

these hot electrons. If the light source is pulsed, then the electron TOF can be used to stop the energetic electrons [19,32]. However, this only works when the electrons are extracted with low electric fields (e.g., <2 V/cm). Besides, our light source is not pulsed. A second solution is the use of an electrostatic energy analyzer to stop the energetic electrons [19]. This only works when the electric field is even lower than in the TOF discrimination. This is because the voltage drop across a finite photoionization region will deteriorate the resolution. For instance, a 1 V/cm electric field would result in a 0.2 eV resolution, if the ionization region were 2 mm thick. The ultimate solution may be the use of an imaging detector in which all electrons are collected in coincidence with the ions [33–35]. With an assumption of an isotropic distribution of electron ejection angles, the data can be inverted so that the portion of the electron signal contributing to the zero electron signal background can be subtracted. Alternatively, a very simple solution may be to collect only two signals, the zero energy coincidences with their ca 5% hot electron contribution, and the coincidence signal associated with energetic electrons that appear in a ring around the central peak. By subtracting the latter from the former normalized to the same collection area, a pure zero energy PEPICO spectrum may emerge. Such an approach would permit PEPICO experiments to be performed with continuous light sources with no hot electron contribution. This method for subtraction of "hot" electrons is a spatial analog of a TOF approach used by Baer and co-workers [36] in which the electrons were pulsed out of the ionization region and the true zero energy electrons were obtained by subtracting the hot electrons appearing at a different TOF region from the TOF region associated with the zero energy electrons.

Acknowledgements

We are grateful for many fruitful discussions about velocity imaging with Paul M. Guyon, Darcy Peterka, Musa Ahmed, and Arthur Suits. We thank Judith Sztaray for carrying out the SIMION calculations. We acknowledge the generous support of this research by the U.S. Department of Energy.

References

[1] J. Dannacher, H.M. Rosenstock, R. Buff, A.C. Parr, R. Stockbauer, R. Bombach, J.P. Stadelmann, Chem. Phys. 75 (1983) 23.
[2] P.R. Das, T. Nishimura, G.G. Meisels, J. Phys. Chem. 89 (1985) 2808.
[3] T. Nishimura, Q. Zha, G.G. Meisels, J. Chem. Phys. 87 (1987) 4589.
[4] K. Norwood, A. Ali, C.Y. Ng, J. Chem. Phys. 95 (1991) 8029.
[5] L.M. Duffy, J.W. Keister, T. Baer, J. Phys. Chem. 99 (1995) 17862.
[6] R. Thissen, C. Alcaraz, J.W. Hepburn, M. Vervloet, O. Dutuit, Int. J. Mass Spectrom. 199 (2000) 201.
[7] K.M. Weitzel, J. Mähnert, H. Baumgärtel, Ber. Bunsenges. Phys. Chem. 97 (1993) 134.
[8] K.M. Weitzel, J. Mähnert, Z. Phys. Chem. 195 (1996) 181.
[9] Y. Li, B. Sztaray, T. Baer, J. Am. Chem. Soc. 123 (2001) 9388.
[10] T. Baer, W.B. Peatman, E.W. Schlag, Chem. Phys. Lett. 4 (1969) 243.
[11] T. Hsieh, J. Gilman, M. Weiss, G.G. Meisels, P.M. Hierl, Int. J. Mass Spectrom. Ion. Proc. 36 (1980) 317.
[12] R. Spohr, P.M. Guyon, W.A. Chupka, J. Berkowitz, Rev. Sci. Instrum. 42 (1971) 1872.
[13] F. Merkt, P.M. Guyon, J.W. Hepburn, Chem. Phys. 173 (1993) 479.
[14] F. Merkt, P.M. Guyon, J. Chem. Phys. 99 (1993) 3400.
[15] G.K. Jarvis, Y. Song, C.Y. Ng, Rev. Sci. Instrum. 70 (1999) 2615.
[16] G.K. Jarvis, K.M. Weitzel, M. Malow, T. Baer, Y. Song, C.Y. Ng, Phys. Chem. Chem. Phys. 1 (1999) 5259.
[17] G.K. Jarvis, K.M. Weitzel, M. Malow, T. Baer, Y. Song, C.Y. Ng, Rev. Sci. Instrum. 70 (1999) 3892.
[18] R.I. Hall, G. Dawber, A. McConkey, M.A. MacDonald, G.C. King, Phys. Rev. Lett. 68 (1992) 2751.
[19] M. Hochlaf, H. Kjeldsen, F. Penent, R.I. Hall, P. Lablanquie, M. Lavollee, J.H.D. Eland, Can. J. Phys. 74 (1996) 856.
[20] D.W. Chandler, M.H.M. Janssen, S. Stolte, R.N. Stickland, J.W. Thoman, D.H. Parker, J. Phys. Chem. 94 (1990) 4839.
[21] D.W. Chandler, D.H. Parker, Adv. Photochem. 25 (1999) 59.
[22] D.A. Dahl, SIMION 3D Version 6.0, Ref Type: Computer Program, Scientific Instrument Services Inc., NJ, 1995.
[23] D.r. Cooper, D. Cubric, D.B. Thompson, P. Bolognesi, M.C.A. Lopes, G.C. King, J. Electron Spectrosc. Relat. Phenom. 112 (2000) 129.
[24] M.E. Gellender, A.D. Baker, Int. J. Mass Spectrom. Ion. Phys. 17 (1975) 1.
[25] T. Baer, in: M.T. Bowers (Ed.), Gas Phase Ion Chemistry, Academic Press, New York, 1979, pp. 153–196.
[26] K.M. Weitzel, M. Malow, G.K. Jarvis, T. Baer, Y. Song, C.Y. Ng, J. Chem. Phys. 111 (1999) 8267.
[27] K.M. Weitzel, G.K. Jarvis, M. Malow, T. Baer, Y. Song, C.Y. Ng, Phys. Rev. Lett. 86 (2001) 3526.

[28] Y. Song, X.-M. Qian, K.C. Lau, C.Y. Ng, J. Chem. Phys. 115 (2001) 4095.
[29] J.B. Pedley, R.D. Naylor, S.P. Kirby, Thermochemical Data of Organic Compounds, Chapman and Hall, London, 1986.
[30] D.D. Wagman, W.H.E. Evans, V.B. Parker, R.H. Schum, I. Halow, S.M. Mailey, K.L. Churney, R.L. Nuttall, The NBS Tables of Chemical Thermodynamic Properties, J. Phys. Chem. Ref. Data 11 (Suppl. 2), US Government Printing Office, NSRDS, Washington, 1982.
[31] K. Walter, R. Weinkauf, U. Boesl, E.W. Schlag, J. Chem. Phys. 89 (1988) 1914.
[32] P.M. Guyon, T. Baer, L.F.A. Ferreira, I. Nenner, A. Tabche-Fouhaile, R. Botter, T.R. Govers, J. Phys. B: Atom. Molec. Phys. 11 (1978) L141.
[33] J.A. Davies, J.E. LeClaire, R.E. Continetti, C.C. Hayden, J. Chem. Phys. 111 (1999) 1.
[34] J.A. Davies, R.E. Continetti, D.W. Chandler, C.C. Hayden, Phys. Rev. Lett. 84 (2000) 5983.
[35] A. Lafosse, M. Lebech, J.C. Brenot, P.M. Guyon, O. Jagutzki, L. Spielberger, M. Vervloet, J.C. Houver, D. Dowek, Phys. Rev. Lett. 84 (2000) 5987.
[36] B.P. Tsai, T. Baer, M.L. Horowitz, Rev. Sci. Instrum. 45 (1974) 494.